Iranica Journal of Energy and Environment
Journal Homepage: www.ijee.net
IJEE an official peer review journal of Babol Noshirvani University of Technology, ISSN:2079-2115

The Effect of Magnetic Field on Non-deposition of Nanoparticles in Microchannels Using Euler-Lagrange Method

N. Hedayati, A. Ramiar*

Faculty of Mechanical Engineering, Microfluidics and MEMs Lab, Babol Noshirvani University of Technology, Babol, Iran

P A P E R I N F O

Paper history:
Received 02 August 2023
Accepted in revised form 21 January 2024

Keywords:
Deposition
Heat transfer
Magnetic field
Microchannels
Nanoparticles

A B S T R A C T

The challenge of particle deposition in microchannels has consistently posed issues in nanofluids, adversely impacting the heat transfer rate. This study investigates the novel approach of employing a magnetic field to prevent deposition and enhance the heat transfer of nanoparticles in microchannels, utilizing Euler-Lagrange method. The analysis involves the coupled solution of momentum and energy equations, incorporating forces such as Brownian motion, thermophoresis, drag, and volumetric force. The findings within the explored parameters indicate that temperature variations affecting particles beyond the thermal boundary layer have a comparatively minor impact compared to those within the boundary layer. This presents an opportunity for optimizing nanoparticle consumption. Additionally, the study reveals that a non-developed flow at the inlet results in lower particle deposition compared to a developed inlet. The results show that an increase in the Reynolds number from 50 to 300 leads to a 1.75% increase in the distance of particles from the wall. The study also delves into the positioning of the current-carrying wire, demonstrating that placing the wire at the microchannel entrance significantly reduces particle deposition. Furthermore, the results indicate that with an increase in electrical current up to 4 amperes, the efficiency of non-deposition reaches 100%.

***Doi**: 10.5829/ijee.2024.15.04.01*

NOMENCLATURE

P	Pressure(P)	f	Fluid
V	Velocity (m/s)	e	Energy
$\boldsymbol{x}$	Length (m)	m	Momentum
t	Time (s)	B	Brownian
Cp	Heat specific capacity (J/(kg K)	D	Drage
F	Force (N)	T	Thermophresis
K_B	Boltzmann Constant (J/K)	g	Gravitational and buoyancy
S	Source term	M	Magnetic
K	Thermal conductivity coefficient (W/m K)	L	Lift
T	Tempreture (K)	**Greek Symbols**	
Subscripts		ρ	Density (kg/m^3)
i , j	Cartesian component	μ	Dynamic viscosity (Pa·s)

INTRODUCTION

Numerous studies have been conducted in the field of microfluidics, nanofluid flow and heat transfer (1-5). It is worth noting that there is limited experimental and numerical work regarding flow in rectangular channels, and most of the referenced papers in this section focus on circular geometries. Many researchers have

*Corresponding Author Email: aramiar@nit.ac.ir (A. Ramiar)

Please cite this article as: Hedayati N, Ramiar, A. The Effect of Magnetic Field on Non-deposition of Nanoparticles in Microchannels Using Euler-Lagrange Method. Iranica Journal of Energy and Environment. 2024; 15(4): 324-37. Doi: 10.5829/ijee.2024.15.04.01

considered nanoparticles as a means to enhance heat transfer rates.

Wang et al. (6) demonstrated that the thermal conductivity coefficient is influenced by microscale motion (Brownian motion and internal particle forces) and particle structure. Lee et al. (7) experimentally investigated the thermal conductivity coefficient of copper oxide and aluminum oxide nanofluid suspensions in water and ethylene glycol. Their results showed that nanofluids exhibit significantly higher thermal conductivity compared to their base fluids. They obtained the effective thermal conductivity coefficient of the nanofluid as a function of the base fluid conductivity coefficient, nanoparticle properties, and their volume fraction. They also reported an almost linear increase in the thermal conductivity coefficient of the nanofluid with increasing nanoparticle volume fraction. They found that the thermal conductivity of copper oxide ethylene glycol nanofluid was 20% higher than the base fluid at a nanoparticle volume fraction of 4%.

Xuan and Li (8) discussed five possible reasons for the improvement of thermal conductivity coefficient of nanoparticles: 1. Increased surface area due to suspended nanoparticles. 2. Increased thermal conductivity of the fluid 3. Interactions and collisions between nanoparticles. 4. Strong mixing and turbulence of the fluid. 5. Dispersion and scattering of nanoparticles.

Keblinski et al. (9) considered four potential mechanisms for the unusually high thermal conductivity coefficient, including: 1. Random motion of nanoparticles. 2. Formation of a layered molecular structure with very high thermal conductivity at the liquid-nanoparticle interface. 3. Nature of heat transfer in nanoparticles. 4. Cluster formation or aggregation of nanoparticles.

Das et al. (10) conducted an experimental investigation on the effect of temperature on thermal conductivity coefficient of nanofluids. They reported a two to threefold increase in this coefficient with temperature in a temperature range of 31 to 51 degrees Celsius. Furthermore, a comparison of the obtained results with equations of Maxwell and Hamilton-Crosser showed that these equations underestimate the thermal conductivity coefficient of nanofluids compared to the actual values.

Khanafer et al. (11) were the first to numerically simulate nanofluid flow. They investigated the natural convection flow of a water-copper mixture in a square cavity. Their results showed that heat transfer and flow velocity of the nanofluid increased compared to the pure fluid due to the increased thermal conductivity coefficient and random motion of nanoparticles.

Wen et al. (12) investigated the laminar convective heat transfer of aluminum oxide water nanofluid in the entrance region of a pipe. Their results showed a 49% enhancement in the Nusselt number for the nanofluid with a volume fraction of nanoparticles of 1.6%. Additionally, the developed region length for the nanofluid was greater than that for the pure fluid, which increased with an increase in the volume percentage of the nanofluid. The particle migration phenomenon, which led to non-uniform enhancement in thermal conductivity and viscosity and resulted in a reduction of the thermal boundary layer, was proposed by them to explain this improvement.

Jalili et al. (13) investigated a two-dimensional nanofluid flow between porous disks under outer magnetic amplitude, employing the Akbari-Ganji Method and Finite Element Method. The study revealed shifting turning points with sliding at the limits, and a reduction in axial velocity with increasing Reynolds number. Contrast in radial velocity profiles identified persistent fluid areas, while heat transmission at the lower porous disk decreased with slip, contrary to the upper plate.

Jalili et al. (14) examined heat transfer in a microchannel heat sink using Aluminum oxide-water nanofluid and considering a magnetic field. They applied the Koo-Kleinstreuer model for nanofluid properties, utilized an improved Darcy relationship for porous medium modeling, and employed the Collocation method to address nonlinearity in heat transfer relationships. Results showed a direct correlation between the magnetic field and Nusselt number, with the highest heat transfer observed at a nanofluid concentration of 0.04%.

Roy et al. (15) investigated the radial laminar flow of aluminum oxide nanofluids in water, ethylene glycol, and oil at different nanoparticle sizes. They reported higher viscosity and lower thermal conductivity for nanofluids with larger particles compared to nanofluids with smaller particles. Additionally, they reported a direct relationship between heat transfer and wall shear stress with Reynolds number and volume fraction of nanoparticles.

Heris et al. (16) investigated the effect of copper oxide-water and aluminum oxide water nanofluids in a pipe with a constant wall temperature. The results showed that the heat transfer rate and wall shear stress were higher compared to base fluids, and increasing the volume fraction of nanoparticles led to an increase in these values. The heat transfer enhancement due to the presence of nanofluids was greater than what is predicted by single-phase fluid equations for heat transfer. They also reported a greater improvement in heat transfer for aluminum oxide water nanofluids compared to copper oxide water nanofluids. Jalili et al. (17) explored thermal aspects of incompressible fluid flow, focusing on non-Newtonian flows with chemical reactions and heat sources, specifically around a stretching sheet. They introduced a novel semi-analytical approach, the Akbari–Ganji method (AGM), alongside the finite element method (FEM). Their findings highlighted the impact of Hartmann number and interaction parameters on velocity profiles, revealing that higher Hartmann numbers decrease fluid velocity and affect temperature values in the studied applications.

He et al (18) investigated the laminar and turbulent flow of TiO_2 nanofluid in water inside a vertical pipe. In this study, three nanoparticles with sizes of 95 nm, 145 nm, and 210 nm were used. The results showed that, at a constant Reynolds number and nanoparticle size, the heat transfer coefficient increases with an increase in the volume fraction of nanoparticles, and the magnitude of heat transfer enhancement is higher in turbulent flow compared to laminar flow. They also reported that, at equal volume fractions and Reynolds numbers, the effect of particle size on heat transfer is small.

Abu-Nada (19) examined heat transfer in a nanofluid flow over a step. He used various nanofluids at different volume fractions. For copper nanoparticles, an improvement was observed in the upper and lower wall regions along the entire path except for the first and second recirculation regions. Outside the recirculation regions, nanoparticles with higher thermal conductivity, such as silver and copper, led to higher Nusselt numbers for larger volume fractions. However, in the recirculation regions, nanoparticles with lower thermal conductivity, such as titanium dioxide, resulted in greater enhancement. Inside the recirculation regions, the Nusselt number was more dependent on the thermal properties of the nanoparticles, while outside these regions, it was also dependent on Reynolds number. Nonetheless, over the entire range of Reynolds numbers considered, increasing the volume fraction led to an increase in the Nusselt number.

Multiphase systems are defined as mixtures of solid, liquid, and gas phases. In this section, we will review some articles written about two-phase flow models. Manninen et al. (20) investigated the governing equations of two-phase flow using the mixture model. They examined previous works related to the mixture model and simplified the governing equations and relationships for the flow. Ultimately, they derived the continuity and momentum equations for the mixture phase and dispersed phase.

Hedayati et al. (21) explored blood flow dynamics in a 3D vessel with two inlets under a magnetic field using OpenFOAM. They found that optimal nanoparticle distribution for drug delivery occurs at lower Reynolds numbers and higher Hartman numbers and temperatures. Adjusting injection angles simultaneously enhances uniformity, and the magnetic field's impact surpasses that of the temperature gradient, becoming more pronounced with increasing Hartman numbers. This study provides insights into factors influencing blood flow and nanoparticle distribution, valuable for drug delivery applications.

Alipanah et al. (22). introduce a magnetophoretic microfluidic device utilizing electroosmotic flow for efficient separation of magnetic particles from human blood. The device features dual channels for blood and buffer, with a central slit guiding particles to the outlet. Integration of a conductive surface creates a flow vortex, collaborating with the magnetic field to overcome drag forces, achieving precise on-chip separation (100 nm to 2.5 µm) by adjusting field strength and electric potential. The device's demonstrated efficacy across varied conditions positions it as a versatile tool for targeting diverse particle-bonded pathogens. Rouson et al. (23) investigated the flow inside a inclined channel using direct numerical simulation and one-way coupling numerical approach. They presented instantaneous images of the particle distribution near the wall and found that small particles tend to settle at very low velocities, while larger particles tend to disperse more uniformly.

Behzadmehr et al. (24) investigated the heat transfer of copper-water nanofluid with a volume fraction of 1% inside a pipe using a two-phase flow model. They examined the effects of turbulence intensity, nanofluid volume fraction, and length of the inlet region on the heat transfer coefficient and Nusselt number in the pipe. They demonstrated that the use of nanofluid improves the heat transfer performance and reported a reduction in the length of the developed flow region when using nanofluid. Furthermore, they mentioned that the effect of turbulence intensity on heat transfer is limited to the inlet region of the flow and diminishes as the flow develops.

Mirmasoumi and Behzadmehr (25) and Akbarinia and Laur (26) numerically investigated the forced convective heat transfer of laminar nanofluid flow inside a pipe. In both studies, they stated that heat transfer increases with a decrease in particle diameter. Kurowski et al. (27) examined three different models, including the homogeneous model, Eulerian-Lagrangian method, and mixture method, for numerically simulating the flow inside a mini-channel. They obtained nearly identical results for all the models.

Lotfi et al. (28) employed the Eulerian two-phase method for the first time to model the behavior of aluminum oxide-water nanofluid inside a pipe. They compared the results obtained from this method with those from single-phase models, the mixed two-phase model, and experimental data, demonstrating that the model proposed by them exhibits satisfactory performance in solving nanofluid flow.

Convective heat transfer of quiescent forced water-copper nanofluid inside a microchannel with uniform heat flux was numerically investigated by Kalteh et al. (29) using the Eulerian-Eulerian model. They concluded that the relative velocities and temperatures between the phases are very small and negligible. Therefore, the nanoparticles and base fluid have nearly the same temperature and velocity, and the volume distribution of nanoparticles is uniform. Furthermore, the results showed that the two-phase model provides a higher heat transfer coefficient compared to the single-phase model. Heat transfer increases with increasing Reynolds number, increasing volume fraction of nanoparticles, and decreasing nanoparticle diameter, while pressure drop slightly increases.

Akbari et al. (30) compared various single-phase models with three two-phase models (VOF, mixture, and Eulerian) for mixed convective heat transfer of water-aluminum oxide nanofluid inside a horizontal pipe. The results showed that the velocity field was nearly the same for different methods, while the temperature field varied. Furthermore, the comparison of the models revealed that although the two-phase models were closer to the experimental results, they overpredicted the heat transfer coefficient compared to the experimental values. They stated that for a better comparison of these models, more experimental data under different flow conditions are needed. Additionally, applying different models to calculate the properties of the nanofluid in these models can also lead to different results.

Bianco et al.(31) investigated forced convection of a nanofluid with Al_2O_3 nanoparticles in turbulent flow regime inside a pipe with constant wall temperature. They used the mixture two-phase model for simulation. They found that increasing the volume fraction of nanoparticles and the Reynolds number would result in an increase in the heat transfer rate.

Rahimi-Esbo et al. (32) numerically investigated the transient flow and heat transfer modeling of forced convection of a nanofluid in a confined jet inside a channel, considering the non-uniform particle distribution. The results of studying the flow and heat transfer parameters of the nanofluid showed that with increasing Reynolds number, aspect ratio, sinusoidal wave amplitude, and volume fraction of nanoparticles, the average Nusselt number would increase. The investigations revealed that with an increase in the aspect ratio, the jet penetration inside the channel becomes more significant, and the flow development length inside the channel increases. A similar effect was observed with increasing the Reynolds number. Furthermore, the investigations demonstrated that with increasing Reynolds number and aspect ratio, the length of the vortex region and flow recirculation also increased. That has directly impact on the increase in local Nusselt number and, consequently, the average Nusselt number. Additionally, the results indicated that the mixture two-phase model exhibited higher heat transfer compared to single-phase models and showed better agreement with experimental results.

Wang et al. (33) explored the impact of geometric parameters on flow and heat transfer in microchannel heat sinks. Numerical simulations, considering water viscosity variation, showed good agreement with experimental data. High aspect ratio rectangular microchannels exhibit the best performance with low thermal resistance. Increasing the number of channels reduced thermal resistance but increased pressure drop, with an optimal range for channel number at the same power consumption.

Alrashed et al .(34) investigated on laminar flow and heat transfer of water-based nanofluids containing multi-walled carbon nanotubes. Different weight percentages and Reynolds numbers were analyzed in a two-dimensional backward-facing contracting channel. Results had shown that increasing Reynolds number and nanoparticle weight percentage improved heat transfer and reduced surface temperature. Higher fluid momentum had led to enhanced axial velocity and potential vortex generation. This behavior had increased velocity gradients and pressure drop at the channel inlet. Increasing nanoparticle mass fraction had improved the average Nusselt number without significant changes in pumping power and pressure drop at high Reynolds numbers, indicating improved thermal efficiency.

Sandeep et al. (35) highlighted the potential of graphene as a promising nanomaterial with continuous electrical conductivity. The investigation focused on the electrically conducting liquid film flow of water-based non-Newtonian nanofluids infused with graphene nanoparticles, which revealed enhanced thermal conductivity in comparison to other nanofluids. A mathematical model was developed for the study, taking into account various parameters and the presence of a transverse magnetic field, and it provided valuable insights into the flow and heat transfer characteristics. The findings emphasized the significant impact of the Deborah number on convective heat transfer; thus, emphasizing the importance of relaxation time in such systems.

Sandeep et al. (36) investigated the impact of extrinsic magnetic fields on the thermal and physical properties of magnetic-nanofluids, as well as their flow and heat transfer characteristics. By considering a transverse magnetic field and variable heat source/sink, the researchers examined the liquid film flow of magnetic-nanofluids near a thin elastic sheet. The numerical analysis, conducted using an R-K based shooting technique, revealed that water-AA 7075 exhibited a significantly higher heat transfer rate compared to water-AA 7072. Furthermore, an increase in the percentage of Cu was found to enhance the heat transfer rate.

Daniel et al. (37) examined the magnetohydrodynamics (MHD) flow of nanofluid towards a nonlinear stretched surface with variable thickness in the presence of an electric field. The analysis included considerations of viscous dissipation, Joule heating, and chemical reaction. The effects of the electric field and variable thickness on heat transfer characteristics were investigated. They revealed a reduction in skin friction, heat, and mass transfer with increasing wall thickness. The electric field was found to enhance nanofluid velocity and temperature while reducing concentration. Thermal radiation was sensitive to nanofluid temperature and thermal boundary layer

thickness. Their results were compared with available data in the limiting case, showing good agreement.

Maleki et al. (38) investigated heat transfer and fluid flow of a pseudo-plastic non-Newtonian nanofluid over a permeable surface with injection and suction. Similarity solution and numerical methods were employed to solve the governing equations. Various nanoparticles and base fluid were considered. The effects of power-law index, nanoparticle volume fraction, nanoparticle type, and permeability were analyzed. The results showed different behaviors in flow and heat transfer for non-Newtonian nanofluids under suction and injection. For injection and impermeable plate, non-Newtonian nanofluids exhibited improved heat transfer compared to Newtonian nanofluids. However, the type of nanoparticles had a stronger influence on heat transfer during suction. Additionally, it was observed that the use of non-Newtonian nanofluids decreased heat transfer in all cases during injection, in contrary to the other two scenarios.

Lin et al. (39) studied the flow and heat transfer of MHD pseudo-plastic nanofluid over an unsteady stretching surface with internal heating effects. Different nanoparticles and a pseudo-plastic base fluid were considered. The effects of power law viscosity on temperature fields were analyzed. The governing equations were solved numerically, and the influence of various parameters on velocity and temperature fields was examined.

Darbari and Ayani (40) investigated the use of nanofluids and baffles to improve heat transfer in a constant heat flux channel. The effects of parameters such as baffle height, baffle spacing, Reynolds number, and concentration of nanoparticles were analyzed. The results showed that increasing the baffle height improved the Nusselt number but increased nanoparticle deposition. Similarly, decreasing the baffle spacing had a positive impact on the Nusselt number and deposition. Vortexes were observed after each baffle, with lower particle concentration. Additionally, particle deposition on baffles was significantly higher than on channel walls.

Numerous studies and investigations have been conducted on heat transfer in microchannels, the role of nanoparticles and various fluids, the influence of magnetic fields on enhancing heat transfer in microchannels, as well as particle deposition and methods to prevent it separately. However, simultaneous studies and investigations on the impact of nanoparticles on heat transfer, the examination of particle deposition, the role of magnetic fields in heat transfer, and prevention of particle deposition through magnetic forces have not been carried out. In this paper, all the important forces in microchannel flow are considered, including thermophoresis force, Brownian force, solving momentum conservation equations, solving energy conservation equations, and taking into account the small particle and channel dimensions.

The Eulerian-Lagrangian method amalgamates the strengths of Eulerian and Lagrangian approaches, offering distinct advantages over methods such as the pure Eulerian approach. In the Eulerian framework, fluid dynamics is described with fixed points in space, while the Lagrangian method tracks the motion of individual fluid particles. This method excels in accurately representing complex fluid phenomena, particularly in scenarios involving intense deformation, fragmentation, or large-scale fluid-structure interactions. By tracking the motion of discrete particles within the Eulerian grid, the approach adeptly handles scenarios with significant fluid distortion, circumventing numerical diffusion issues associated with Eulerian methods. The Eulerian-Lagrangian approach is well-suited for simulations involving fluid-solid interactions, multiphase flows, and scenarios where precise particle trajectory representation is crucial for understanding and predicting fluid behavior. In this paper, the choice of the Eulerian-Lagrangian method is motivated by its capability to accurately capture natural particle behavior at the microscopic level. The subsequent discussion focuses on the deposition and heat transfer mechanisms of nanoparticles in microchannels. Results guide improvements, addressing methods to enhance heat transfer, including the impact of magnetic fields and other techniques. The dominant Reynolds number for solving problems with a volume fraction of 0.3% for nanofluids is approximately 100.

GOVERNING EQUATIONS

Continuous phase

The governing equations for the continuous phase fluid are as follows:

$$div(\rho_f V_f) = 0 \quad [1]$$

$$\rho_f \left(\frac{\partial (V_f)_i}{\partial t} + (V_f)_j \frac{\partial (V_f)_i}{\partial x_j}\right) = -\frac{\partial P}{\partial x_i} + \mu_f . \frac{\partial^2 (V_f)_i}{\partial x_j^{\,2}} + \rho_f . (S_m)_i \quad [2]$$

$$\rho_f C_p \left(\frac{\partial T}{\partial t} + (V_f)_i . \frac{\partial T}{\partial x_i}\right) = k_f \frac{\partial^2 T}{\partial x_i^{\,2}} + (S_e)_i \quad [3]$$

In Equations 1-3, the terms S_m, ρ_f, V_f, C_p, μ_f, T, S_e, k_f, represents the momentume source term, fluid density, velocity, specific heat capacity, viscosity, temperature, energy source term, and thermal conductivity respectively. The momentume source term indicating the continuous transfer between the fluid and the particle phase over the passage time of particles through the control volume. For the fluid phase, it is expressed as Equation 4.

$$S_m = \sum_{np} \frac{m_p}{\partial V} \vec{F} \quad [4]$$

where δV represents the cell volume, np is the number of particles inside the control volume, and cells with $np = 0$ are considered to have a value of zero for the source term. $\vec{F}$ represens the sum of forces acting on the particle.

Discrete phase

The equation of motion for a particle using second law of Newton is as follows:

$$\frac{d\vec{X}_p(x,y)}{dt}=\vec{V}_p \quad [5]$$

$$\frac{d\vec{V}_p}{dt}=\vec{F}_D+\vec{F}_B+\vec{F}_T+\vec{F}_g+\vec{F}_M+\vec{F}_L \quad [6]$$

where F_D, F_B, F_T, F_g, F_M, and F_L represent the drag force, Brownian force, thermophresis force, gravitational and buoyancy force, magnetic force, and lift force, respectively and Index P represents the particle.

Drag force (F_D)

The drag force (F_D) is the force exerted on a particle due to the relative velocity between the particle and the fluid. Particularly, when the Reynolds number is less than 100, the drag force is the dominant force governing the motion of the particle. The drag force can be determined using Equation 7.

$$F_D=\frac{\pi}{8}\rho_f d_p{}^2 C_D\left(V_f-V_p\right)^2.\frac{\left(V_f-V_p\right)}{\left|V_f-V_p\right|} \quad [7]$$

The Reynolds number of the particle, denoted as Re_p, is defined as follows:

$$\mathrm{Re}_p=\frac{\rho_f d_p\left|V_f-V_p\right|}{\mu_f} \quad [8]$$

The drag coefficient, C_D, is defined based on different regimes: Stokes' Law (for Rep < 1), Modified Stokes' Law (for 1 < Rep < 500), and Newton's Law (for 500 < Rep < 2×105), as follows:

$$\begin{cases} C_D=\dfrac{24}{\mathrm{Re}_p} & \mathrm{Re}_p<1 \\ C_D=1+\dfrac{24}{\mathrm{Re}_p}(1+0.15\mathrm{Re}_p^{0.687}) & 1<\mathrm{Re}_p<500 \\ C_D=0.44 & \mathrm{Re}_p>500 \end{cases} \quad [9]$$

The relaxation time of a particle is the time required for the particle to respond to changes in the fluid velocity. It is defined as follows:

$$\tau=\frac{\rho_p d_p^2}{18\mu_f} \quad [10]$$

Magnetic force (F_M)

Permanent magnets and electromagnets at microscopic dimensions can generate a magnetic field large enough (greater than 0.5 Tesla) to magnetically saturate electromagnetic particles. In this state, the particles act like permanent magnets. Calculating the magnetic field acting on a particle involves various sources and equations depending on the type of field, particle size, and other parameters. Figure 1 illustrates a representation of the magnetic field acting on a particle around an electric current-carrying wire.

The following equation is used to calculate the magnetic force acting on a particle (41)

$$F_m=\iiint_V \mu_0 M.\nabla H dV \quad [11]$$

Brownian force (F_B)

It is created by the random collision of particles with fluid molecules. Brownian force can be significant for particles smaller than a micrometer. Especially in the vicinity of a wall (solid surface) where turbulence intensity is negligibly small, Brownian force is the mechanism for particle motion transfer. This force is determined as follows:

$$F_{Bi}=\zeta_i\sqrt{\frac{\pi S_0}{\Delta t}} \quad [12]$$

ξ_i is an independent Gaussian random variable with zero mean and unit variance. The components of the Brownian force are modeled during the white Gaussian noise process with spectral intensity Sn_{ij} (41).

$$S_{n,ij}=S_0\delta_{ij}$$

$$S_0=\frac{216\nu K_B T}{\pi^2\rho_l d_p^5(\frac{\rho_p}{\rho_l})^2 C_c} \quad [13]$$

where υ is the dynamic viscosity and K_B is the Boltzmann constant.

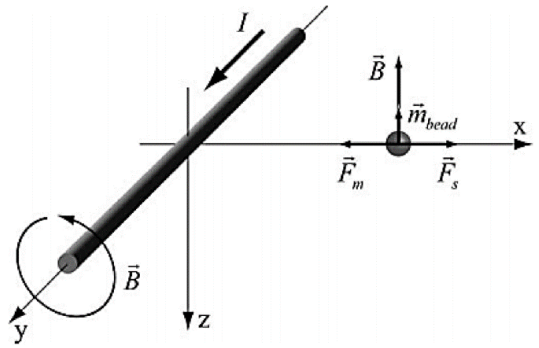

Figure 1. Schematic of a particle moving around a current-carrying wire (41)

Thermophoretic force (F_T)

When a particle exists in a temperature gradient within a flow field, another force called thermophoretic force acts on the particle, which is generated through momentum exchange between the particle and the fluid. Higher molecular velocities on one side of the particle, due to higher temperatures, lead to increased momentum exchange and result in a force in the direction of temperature reduction. In other words, particles are dispersed under the influence of temperature gradients. The thermophoretic force is expressed as follows (41).

$$F_T = -D_{T,p}\frac{1}{m_p T}\nabla T \quad [14]$$

where $D_{T,p}$ is the thermophoretic constant, which is defined as follows:

$$F_T = -\frac{6\pi d_p \mu_f^2 C_s (k + C_t kn)}{\rho_f (1+3C_m kn)(1+2k+2C_t kn)}\frac{1}{m_p T}\nabla T \quad [15]$$

where $C_m = 1.146$, $C_s = 1.147$, $C_t = 2.18$ are the exchange coefficient, thermal slip coefficient, and thermal jump coefficient, respectively. Additionally, *K* represents the ratio of the fluid thermal conductivity coefficient to the particle's, and *Kn* is the Knudsen number, defined as follows:

$$kn = \frac{2\lambda}{d_p} \quad [16]$$

where λ is the mean free path distance of fluid molecules.

Gravitational and Buoyancy force (Fg)

These forces are only significant for large particles in the Stokes regime and are expressed as follows:

$$F_g = (1-\frac{\rho_f}{\rho_p})\, g \quad [17]$$

Deposition of particles

When a particle collides with a surface, it essentially undergoes deformation. The contact area between particles and the surface plays a crucial role in particle adhesion to the surface. The adhesive force is calculated based on the particle size and material properties using constants extracted from experimental data. The adhesive force, as given by Soltani and Ahmadi (42), is calculated as follows:

$$F_{po} = k_s W_A d_p \quad [18]$$

where k_s is a constant equal to $3\pi/4$ The adhesive work, W_A, is a material and particle-specific constant with units of J/m^2 This constant is obtained from experimental data for certain materials. For each particle, the coefficient of restitution represents the ratio of the reflected velocity to the normal velocity of the particle. When the normal collision velocity is relatively high, the coefficient of restitution remains relatively constant. However, as these velocities decrease, the importance of adhesive force increases, leading to a significant decrease in the reflected velocities. In other words, as the normal velocity of the particle decreases, the reflected velocity decreases and eventually reaches a point where no further rebound occurs, and all particles become deposited. This velocity at which particle deposition occurs is called the critical/sticking velocity.

Branch and Dunn (43) proposed an expression for calculating the stopping velocity of a particle using a semi-empirical model, which has been utilized in this paper.

$$v_{cr} = (\frac{2E}{d_p})^{10/7} \quad [19]$$

The composite modulus of Young is called E modulus and is determined based on the modulus of Young of the particle. The normal velocity of the particle (v_n) is compared to the stopping velocity. If the normal velocity of the particle is lower than the stopping velocity, the particle adheres to the surface, otherwise it separates from the surface.

$v_{cr} > v_n$ The particle adheres to the surface.

$v_{cr} < v_n$ The particle separates from the surface.

When the particle separates, it continues its trajectory until it leaves the region or re-impacts the surface. The composite modulus of Young is determined by the following equations:

$$E = 0.51[\frac{5\pi^2 (k_1 + k_2)}{4\rho_p^{3/2}}]^{2/5} \quad [20]$$

$$k_1 = \frac{(1-v_s^2)}{\pi E_s} \quad [21]$$

$$k_2 = \frac{(1-v_p^2)}{\pi E_p} \quad [22]$$

where E_s is the surface modulus of Young in pascals, v_s is the surface ratio of Poisson, E_p is the particle modulus of Young in pascals, v_p is the particle ratio of Poisson, and d_p and d_p respectively represent the density and diameter of the particle.

Equations of particle temperature

The energy equation for spherical particles is expressed as follows according to Ounis et al. (44)

$$\rho_p C_{p_p}\frac{dT_p}{dt} = \frac{6h}{d}(T - T_p) \quad [23]$$

Furthermore, the energy source term, S_e, is included in Equation 23 for the energy equation as follows:

$$S_e = \sum_{np} \frac{m_p}{\delta V} C_p . \frac{dT_p}{dt} \qquad [24]$$

GEOMETRY AND BOUNDARY CONDITIONS

This paper investigates three geometries known as simple microchannel geometry, cavity geometry, and obstacle geometry to investigate particle deposition in microchannel. Figure 2 and Table 1 show schematic of geomeries characteristics of microchannel.

The first geometry, Figure 2a, relates to the geometry of a simple 2D channel. The inlet velocity condition and the outlet pressure condition have been considered. A constant flux of 200,000 watts per square meter is applied to the lower wall according to Vanaei et al. (3), and the upper wall is assumed to be adiabatic and these conditions hold for two other geometries as well.

In the second geometry, Figure 2b, three obstacles are placed according to Husain and Kim (45). This geometry has been chosen to generate a higher volume fraction of particles in the lower wall at the beginning of the channel. Then, in the second obstacle, they are directed towards the cold region and cooled down. In the third obstacle, the cooled particles are directed towards the hot region to generate a higher heat transfer due to the significant temperature gradient. Additionally, the presence of vortexes in the channel can create higher heat transfer compared to a simple channel.

The third geometry, Figure 2c, is derived from Xia et al. (46). This geometry features symmetrical dual triangular cavities. This type of geometry reduces pressure drop compared to the internal obstacle and also enhances heat transfer due to the generation of vortices in the microchannels. Furthermore, this geometry can create a more uniform heat distribution along the channel, leading to an increased number of effective particles in the channel. The selected triangles are right triangles with a chosen acute angle of 30 degrees.

VALIDATION

Figure 3 shows the validation of the Eulerian-Lagrangian model through laboratory experimentation (47), the relevant geometry pertains to a three-dimensional channel with a circular cross-section.

Figures 4 and 5 demonstrate the validation of the effect of the magnetic field as presented by Bali et al. (48).

Table 1. Geometric specifications

L(*mm*)	W(*μm*)	W1 (*μm*)	W2 (*μm*)
1	180	40	40

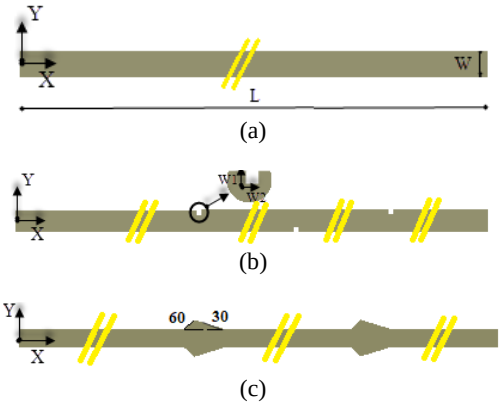

Figure 2. Schematic of geomeries, (a) simple (b) obstacle, and (c) cavity microchannel

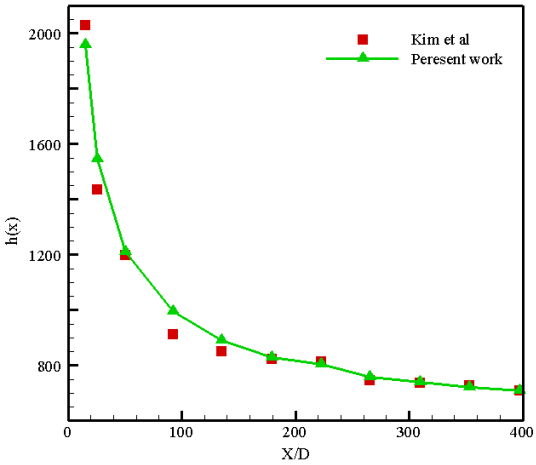

Figure 3. Validation plot of the new method through laboratory experimentation (47)

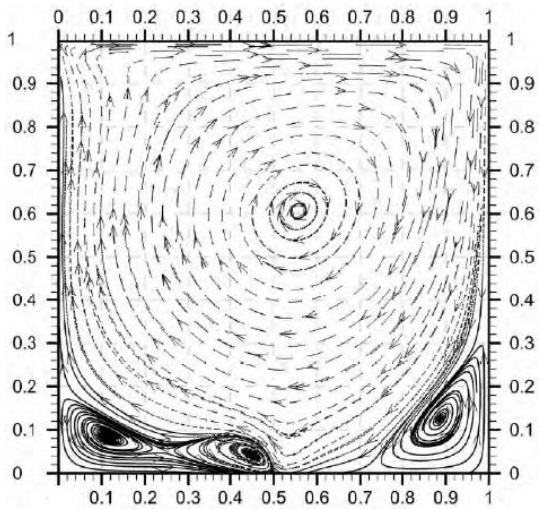

Figure 4. Velocity contour in the cavity under the influence of a magnetic field (48)

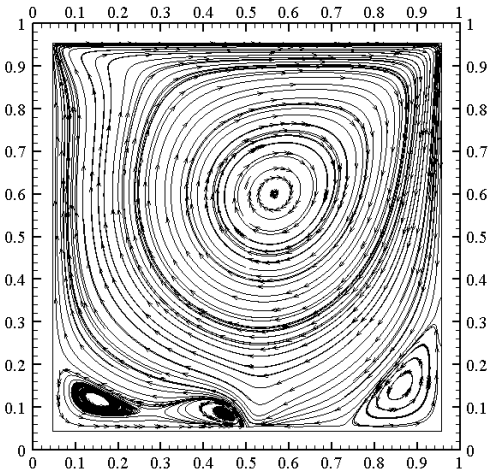

Figure 5. Velocity contour in a cavity under the influence of a magnetic field in the new work

RESULT AND DISCUSSION

The microscopic mechanism of particle deposition in microchannels

As shown in Figures 6 and 7, deposition in microchannels can occur simultaneously at the top and bottom of the microchannel. Factors contributing to this phenomenon include channel geometry, the presence of relatively strong Brownian and thermophoresis forces, small particle size, and the lack of developed flow and uniform flow at the inlet of the microchannel. This means that the presence of undeveloped or uniform flow at the microchannel inlet, and consequently the velocity gradient perpendicular to the wall surface, results in a higher deposition of particles at the beginning of the channel. As the flow becomes more developed, the maximum velocity in the middle of the channel increases. This increase in particle velocity can play a key role in particle deposition.

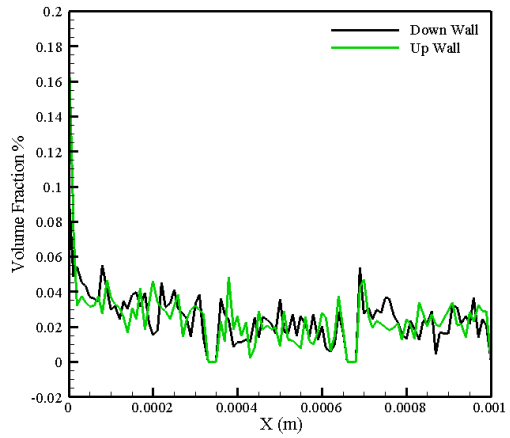

Figure 6. Particle deposition in a two-dimensional microchannel with triangular indentations at Reynolds 100

For microchannels where nanofluid enters from the inlet (the entire inlet area is filled with nanofluid) and the inlet of the microchannel is developed, particle deposition is evident in the simple microchannel. However, if the inlet flow enters the channel in an undeveloped form, deposition will not be noticeable. Figures 8 to 10 When the flow enters the microchannel in an undeveloped form, the velocity gradient created due to the no-slip condition causes particles near the microchannel wall to move diagonally towards the center of the channel. As the particle continues its motion, it experiences a decrease in the intensity of the velocity gradient near the wall (approaching developed flow), resulting in a reduction in the concentration of motion towards the center. This mechanism continues until the particles are no longer subject to the velocity gradient caused by the no-slip condition and the flow becomes developed. From then on, the particle follows an almost linear and straight trajectory. This straight-line motion is subject to disturbances, oscillations, and vertical movements along the path due to the effects of Brownian and buoyancy forces, thermophoresis, and the weight of the particle. If the magnitude of these forces is large, particles will deposit in the channel, while if it is small, deposition will occur less frequently. Therefore, it can be said that undeveloped inlet flows in the channels are at least

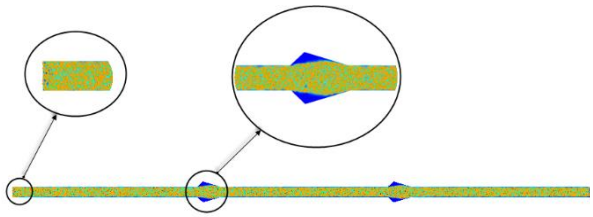

Figure 7. Particle deposition in three sections of a two-dimensional microchannel with triangular indentations

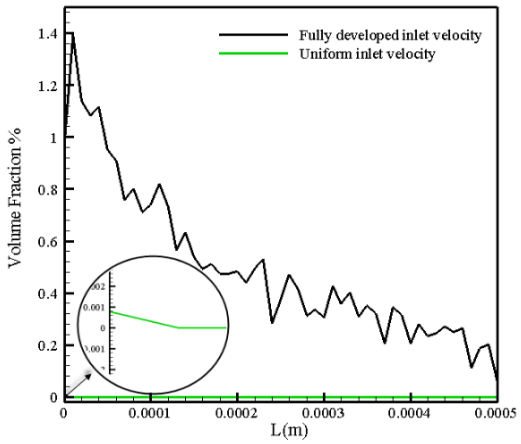

Figure 8. Volume fraction of particles in two conditions of developed and undeveloped inlet flow in a simple two-dimensional channel at Reynolds flow 100

Figure 9. Particle Deposition in a Simple Microchannel with Developed Inlet Velocity

Figure 10. Particle Deposition in a Simple Microchannel with Uniform Inlet Velocity

effective in improving the non-deposition of nanoparticles in microchannels.

Heat transfer of nano particles in a simple two-dimensional microchannel

With the entry of particles into the thermal boundary layer of the fluid, the mechanism of heat transfer becomes effective in nanofluids. Upon entering this region of the fluid, the temperature gradient of the fluid increases near the wall, leading to an enhancement in fluid heat transfer. Therefore, the presence of particles in geometries that lack a minimum two-sided thermal input (in other words, heat enters the fluid from only one wall) outside the thermal boundary layer is either useless or at least very less useful. Figure 11 This aspect can be important in optimizing the particle consumption in the fluid. With the movement of particles in microchannels, the effective temperature effect of the particles is greater at the beginning of the microchannels than at their end. With the movement of particles in the thermal boundary layer, the temperature of the particles consistently increases, effectively reducing the heat absorption capacity of the particle. On the other hand, the presence of volumetric fraction in the initial walls of microchannels increases due to the undeveloped flow. These factors contribute to a greater improvement in non-uniformity at the beginning of the microchannel compared to the improvement at the end of the channel.

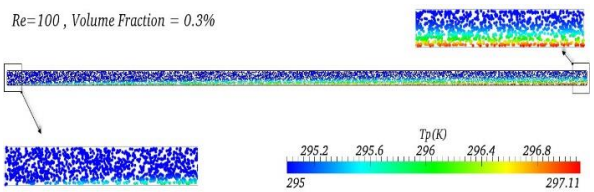

Figure 11. Thermal effects of particles inside and outside of the microchannel

Simple microchannel

Since deposition in microchannels occurs less in non-developed flow conditions compared to developed flow conditions, all flows are examined and evaluated assuming uniform flow at the inlet. As shown in Figure 8 to 10, deposition reaches its minimum value in a simple microchannel, but the presence of particles in a region further away from the lower wall reduces the effectiveness of nanoparticles. Therefore, both parameters need to be considered together to reach an optimal conclusion.

Considering the mentioned factors, one of the methods to control particle deposition is creating higher velocity gradients at the inlet of the microchannel. One way to create this gradient is by increasing the inlet velocity. Figure 11 illustrates the movement of particles near the wall at Reynolds numbers of 50, 100, 200, and 300. This figure shows that as the particle velocity increases, the particle is positioned further away from the microchannel walls. As evident from Figure 12, as the Reynolds number increases, the distance between the nearest particle and the wall increases, resulting in less deposition of particles. Particles in Reynolds 300 are situated 1.75% more distant from the lower wall compared to their position in Reynolds 50.

Microchannel with square obstacles

Figures 13 to 15 illustrate particle deposition in a microchannel with square obstacles. Figures 13 and 14 show the first obstacle with less deposition observed horizontal surface of an obstacle, while in the second and third obstacles, a greater amount of deposition is visible due to the movement of particles towards the obstacles.

The deposition of particles in the second and third obstecles is respectively 581.25% and 593.2% higher than that in the first obstecle. Figure 15 illustrates the deposition of particles on the vertical walls of the obstacles. The findings indicate a higher deposition on the

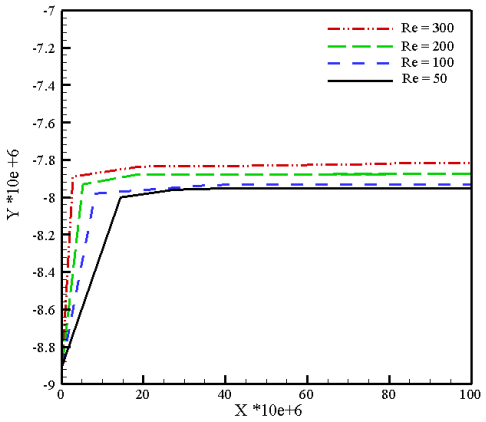

Figure 12. The effect of different Reynolds numbers on the particle distance from the lower wall

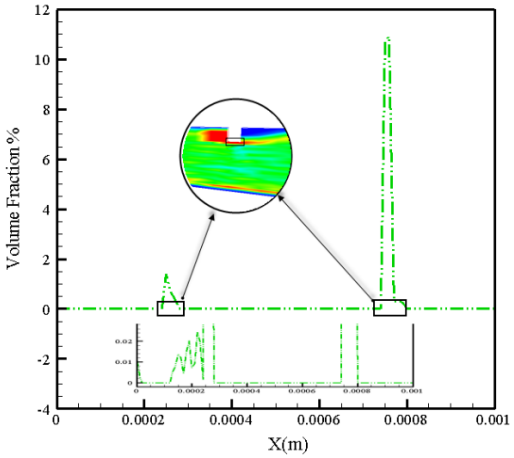

Figure 13. Particle deposition in a microchannel with square obstacles near the upper wall

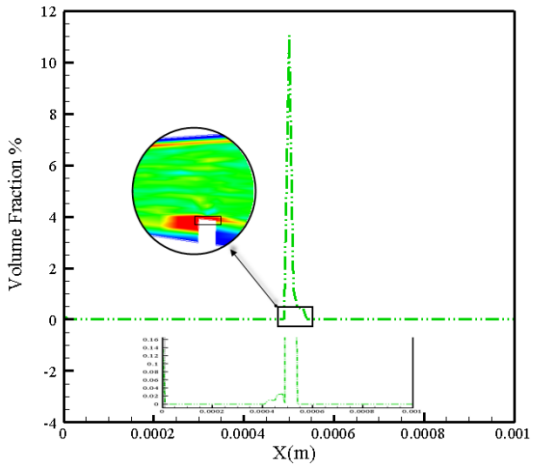

Figure 14. Particle deposition in a microchannel with square obstacles near down wall

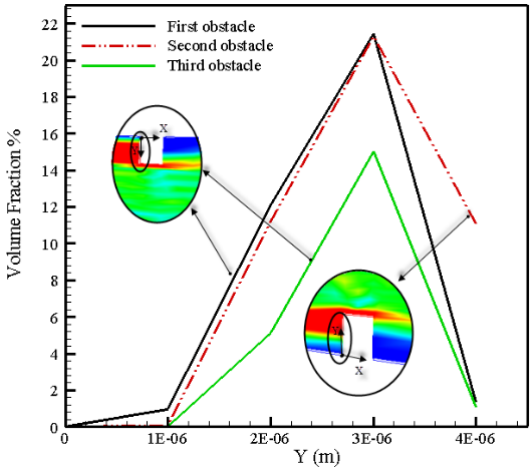

Figure 15. Particle deposition of particles on vertical wall of the obstacles

first obstacle (62.44%) and the second obstacle (88.87%) compared to the third one.

Microchannel with triangular cavities

As shown in Figure 16 the deposition of the particles in a microchannel with triangular cavities is observed globally. This deposition occurs on both the upper and lower walls of the channel. Compared to a simple channel, this channel exhibits a higher concentration of deposition.

The effect of magnetic force on particle deposition

Since particle deposition in microchannels is usually global rather than localized, finding a location where the least number of current-carrying wires can be used and be of significant importance. This importance can have industrial and economic implications in terms of productivity and efficiency. velocity gradients can lift particles to higher positions. More precisely, the point of particle uplift in the flow with undeveloped inlet conditions is close to the channel inlet. Therefore, placing the current-carrying wire at the beginning of the channel path can minimize particle deposition throughout the channel's entire range and reduce it to the minimum possible value.

Figure 17 illustrates the placement of the current-carrying wire and the generation of a certain type of field around the wire, which extends to the entire fluid domain as a result. Figure 18 illustrates the effect of the magnetic field on the temperature variations of particles. As evident from comparing Figures 19 and 20, as the distance of the particle from the wall increases, the heat received by the particle decreases. The magnitude of the magnetic field should be chosen in a way that maximizes heat transfer and minimizes wall deposition.

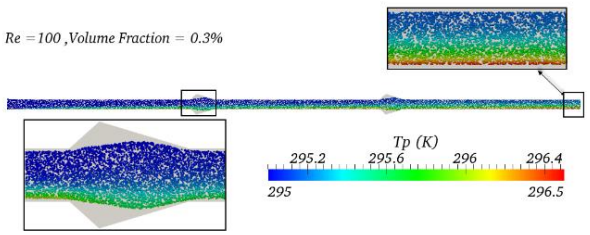

Figure 16. Temperature distribution of particles in microchannel geometry with triangular cavity, Reynolds number 100, volume fraction 0.3%

Figure 17. Placement of the current-carrying wire in a microchannel with triangular cavities

As the current-carrying wire becomes stronger, the particle deposition on the lower wall of the channel decreases. This indicates that an optimal point can be found for this volume fraction. Figure 21 illustrates the influence of four electrical currents (0, 2, 3, 4 Amperes) on generating a magnetic field, thereby deterring particles from depositing on the lower wall and leading to a reduction in particle deposition. As depicted, the effectiveness of deposition prevention rises with an increase in electrical current. It is worth noting that at an electrical current of 4 amperes (I = 4A), the efficiency of non-deposition reaches 100%.

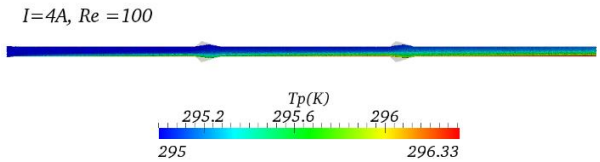

Figure 18. The effect of the magnetic field on the deposition and temperature of particles on the lower wall of a microchannel with triangular cavity

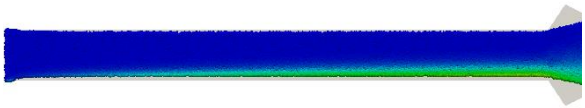

Figure 19. The effect of the magnetic field on the particle deposition in the initial one-third of a microchannel with triangular cavity

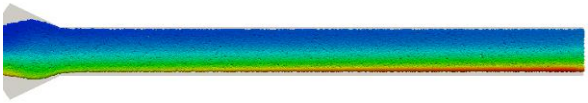

Figure 20. The effect of the magnetic field on the particle deposition in the final one-third of a microchannel with triangular cavity

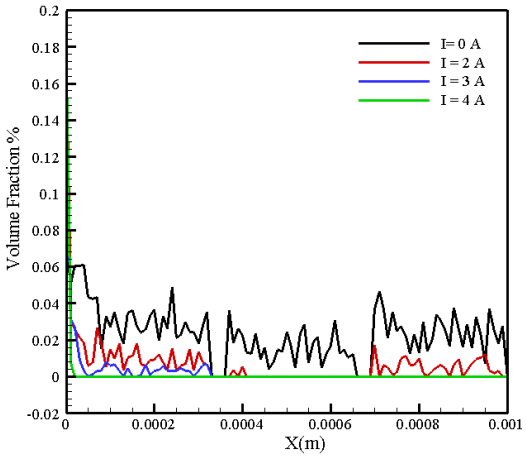

Figure 21. Particle deposition on the bottom wall of a microchannel with triangular cavity under different electric currents

CONCLUSION

This study addressed the persistent challenge of particle deposition in microchannels within nanofluids and its adverse impact on heat transfer rates. The effectiveness of a magnetic field as an innovative solution to prevent deposition and enhance the heat transfer of nanoparticles was explored using the Euler-Lagrange method. Three geometries—simple microchannel, cavity, and obstacle—were examined to analyze particle deposition in microchannels. The findings revealed that the deposition of particles in the second and third obstacles was significantly higher (581.25% and 593.2%, respectively) than in the first obstacle.

The analysis, considering various forces, indicated that temperature variations beyond the thermal boundary layer had a minor impact compared to within the boundary layer, presenting an opportunity for optimizing nanoparticle consumption. The study suggested that undeveloped flow conditions at the microchannel inlet were effective in improving non-deposition of nanoparticles. While heat transfer became effective with particles entering the thermal boundary layer, those near the microchannel entrance experienced a greater temperature effect than those at the end. The study underscored the importance of considering both particle deposition and particle presence away from the lower wall to reach an optimal conclusion.

The study noted that higher Reynolds numbers resulted in particles being positioned further away from microchannel walls, thus reducing deposition. The results showed that particles in Reynolds 300 were positioned 1.75% farther from the lower wall compared to Reynolds 50.

Furthermore, the study demonstrated that by utilizing the magnetic field created by the current-carrying wire, particle deposition could be further reduced. It was observed that increasing the current of the current-carrying wire reduced particle deposition on the lower wall. Notably, at an electrical current of 4 amperes (I = 4A), non-deposition efficiency reached 100%. Due to the significance of the particle deposition issue and the challenges it poses in reality, optimizing electrical current could be considered in the future to achieve suitable efficiency in preventing particle deposition and maximizing heat transfer in various microchannels.

REFERENCES

1. Jalili P, Azar AA, Jalili B, Ganji DD. Study of nonlinear radiative heat transfer with magnetic field for non-Newtonian Casson fluid

flow in a porous medium. Results in Physics. 2023; 48: 106371. Doi: 10.1016/j.rinp.2023.106371

2. Jalili B, Emad M, Jalili P, Ganji DD, Saleem S, Tag-eldin EM. Thermal analysis of boundary layer nanofluid flow over the movable plate with internal heat generation, radiation, and viscous dissipation. Case Studies in Thermal Engineering. 2023: 103203. Doi: 10.1016/j.csite.2023.103203
3. Vanaei P, Jalili B, Hosseinzadeh M, Jalili P. Efficiency Optimization Thermal Analysis and Power Output of a Modified Incinerator Plant Using Organic Rankine Cycle. International Journal of Engineering. 2023; 36(7): 1300-9. Doi: 10.5829/IJE.2023.36.07A.11
4. Hedayati N, Ramiar A. Investigation of two phase unsteady nanofluid flow and heat transfer between moving parallel plates in the presence of the magnetic field using GM. Challenges in Nano and Micro Scale Science and Technology. 2016; 4(1): 52-8. Doi: 10.7508/TPNMS.2016.02.006
5. Hedayati N, Ramiar A, Sedighi K. Investigation of Visco-rheological Properties of Polymeric Fluid on Electrothermal Pumping. Journal of Applied and Computational Mechanics. 2024; 10(1): 164-82. Doi: 10.22055/JACM.2023.44214.4180
6. Wang X, Xu X, Choi SU. Thermal conductivity of nanoparticle-fluid mixture. Journal of thermophysics and heat transfer. 1999; 13(4): 474-80. Doi: 10.2514/2.6486
7. Lee S, Choi S-S, Li S, and, Eastman J. Measuring thermal conductivity of fluids containing oxide nanoparticles. 1999. Doi: 10.1115/1.2825978
8. Xuan Y, Li Q. Heat transfer enhancement of nanofluids. International Journal of heat and fluid flow. 2000; 21(1): 58-64. Doi: 10.1016/S0142-727X(99)00067-3
9. Keblinski P, Phillpot S, Choi S, Eastman J. Mechanisms of heat flow in suspensions of nano-sized particles (nanofluids). International journal of heat and mass transfer. 2002; 45(4): 855-63. Doi: 10.1016/S0017-9310(01)00175-2
10. Das SK, Putra N, Thiesen P, Roetzel W. Temperature dependence of thermal conductivity enhancement for nanofluids. J Heat Transfer. 2003; 125(4): 567-74. Doi: 10.1115/1.1571080
11. Khanafer K, Vafai K, Lightstone M. Buoyancy-driven heat transfer enhancement in a two-dimensional enclosure utilizing nanofluids. International journal of heat and mass transfer. 2003; 46(19): 3639-53. Doi: 10.1016/S0017-9310(03)00156-X
12. Wen D, Ding Y. Experimental investigation into convective heat transfer of nanofluids at the entrance region under laminar flow conditions. International journal of heat and mass transfer. 2004; 47(24): 5181-8. Doi: 10.1016/j.ijheatmasstransfer.2004.07.012
13. Jalili B, Roshani H, Jalili P, Jalili M, Pasha P, Ganji DD. The magnetohydrodynamic flow of viscous fluid and heat transfer examination between permeable disks by AGM and FEM. Case Studies in Thermal Engineering. 2023; 45: 102961. Doi: 10.1016/j.csite.2023.102961
14. Jalili B, Rezaeian A, Jalili P, Ommi F, Ganji DD. Numerical modeling of magnetic field impact on the thermal behavior of a microchannel heat sink. Case Studies in Thermal Engineering. 2023; 45: 102944. Doi: 10.1016/j.csite.2023.102944
15. Roy G, Nguyen CT, Lajoie P-R. Numerical investigation of laminar flow and heat transfer in a radial flow cooling system with the use of nanofluids. Superlattices and Microstructures. 2004; 35(3-6): 497-511. Doi: 10.1016/j.spmi.2003.09.011
16. Heris SZ, Etemad SG, Esfahany MN. Experimental investigation of oxide nanofluids laminar flow convective heat transfer. International communications in heat and mass transfer. 2006; 33(4): 529-35. Doi: 10.1016/j.icheatmasstransfer.2006.01.005
17. Jalili P, Sharif Mousavi S, Jalili B, Pasha P, Ganji DD. Thermal evaluation of MHD Jeffrey fluid flow in the presence of a heat source and chemical reaction. International Journal of Modern Physics B. 2023: 2450113. Doi: 10.1142/S0217979224501133
18. He Y, Jin Y, Chen H, Ding Y, Cang D, Lu H. Heat transfer and flow behaviour of aqueous suspensions of TiO2 nanoparticles (nanofluids) flowing upward through a vertical pipe. International journal of heat and mass transfer. 2007; 50(11-12): 2272-81. Doi: 10.1016/j.ijheatmasstransfer.2006.10.024
19. Abu-Nada E. Application of nanofluids for heat transfer enhancement of separated flows encountered in a backward facing step. International Journal of Heat and Fluid Flow. 2008; 29(1): 242-9. Doi: 10.1016/j.ijheatfluidflow.2007.07.001
20. Manninen M, Taivassalo V, Kallio S. On the mixture model for multiphase flow. VTT Technical Research Centre of Finland. 1996. ISBN (Print): 951-38-4946-5
21. Hedayati N, Ramiar A, Larimi M. Investigating the effect of external uniform magnetic field and temperature gradient on the uniformity of nanoparticles in drug delivery applications. Journal of Molecular Liquids. 2018; 272: 301-12. Doi: 10.1016/j.molliq.2018.09.031
22. Alipanah M, Hafttananian M, Hedayati N, Ramiar A, Alipanah M. Microfluidic on-demand particle separation using induced charged electroosmotic flow and magnetic field. Journal of Magnetism and Magnetic Materials. 2021; 537: 168156. Doi: 10.1016/j.jmmm.2021.168156
23. Rouson DW, Eaton JK. On the preferential concentration of solid particles in turbulent channel flow. Journal of Fluid Mechanics. 2001; 428: 149-69. Doi: 10.1017/S0022112000002627
24. Behzadmehr A, Saffar-Avval M, Galanis N. Prediction of turbulent forced convection of a nanofluid in a tube with uniform heat flux using a two phase approach. International journal of heat and fluid flow. 2007; 28(2): 211-9. Doi: 10.1016/j.ijheatfluidflow.2006.04.006
25. Mirmasoumi S, Behzadmehr A. Numerical study of laminar mixed convection of a nanofluid in a horizontal tube using two-phase mixture model. Applied Thermal Engineering. 2008; 28(7): 717-27. Doi: 10.1016/j.applthermaleng.2007.06.019
26. Akbarinia A, Laur R. Investigating the diameter of solid particles effects on a laminar nanofluid flow in a curved tube using a two phase approach. International Journal of Heat and Fluid Flow. 2009; 30(4): 706-14. Doi: 10.1016/j.ijheatfluidflow.2009.03.002
27. Kurowski L, Chmiel-Kurowska K, Thulliea J. Numerical simulation of heat transfer in nanofluids. Computer Aided Chemical Engineering. 26: Elsevier; 2009. p. 967-72. Doi: 10.1016/S1570-7946(09)70161-0
28. Lotfi R, Saboohi Y, Rashidi A. Numerical study of forced convective heat transfer of nanofluids: comparison of different approaches. International Communications in Heat and Mass Transfer. 2010; 37(1): 74-8. Doi: 10.1016/S1570-7946(09)70161-0
29. Kalteh M, Abbassi A, Saffar-Avval M, Harting J. Eulerian–Eulerian two-phase numerical simulation of nanofluid laminar forced convection in a microchannel. International journal of heat and fluid flow. 2011; 32(1): 107-16. Doi: 10.1016/j.ijheatfluidflow.2010.08.001
30. Akbari M, Galanis N, Behzadmehr A. Comparative analysis of single and two-phase models for CFD studies of nanofluid heat transfer. International Journal of Thermal Sciences. 2011; 50(8): 1343-54. Doi: 10.1016/j.ijthermalsci.2011.03.008
31. Bianco V, Nardini S, Manca O. Enhancement of heat transfer and entropy generation analysis of nanofluids turbulent convection flow in square section tubes. Nanoscale research letters. 2011; 6: 1-12. Doi: 10.1186/1556-276X-6-252
32. Rahimi-Esbo M, Ranjbar A, Ramiar A, Rahgoshay M, Arya A. Numerical study of the turbulent forced convection jet flow of nanofluid in a converging duct. Numerical Heat Transfer, Part A: Applications. 2012; 62(1): 60-79. Doi: 10.1080/10407782.2012.677368

33. Wang H, Chen Z, Gao J. Influence of geometric parameters on flow and heat transfer performance of micro-channel heat sinks. Applied Thermal Engineering. 2016; 107: 870-9. Doi: 10.1016/j.applthermaleng.2016.07.039
34. Alrashed AA, Akbari OA, Heydari A, Toghraie D, Zarringhalam M, Shabani GAS, Seifi AR, Goodarzi M. The numerical modeling of water/FMWCNT nanofluid flow and heat transfer in a backward-facing contracting channel. Physica B: Condensed Matter. 2018; 537: 176-83. Doi: 10.1016/j.physb.2018.02.022
35. Sandeep N, Malvandi A. Enhanced heat transfer in liquid thin film flow of non-Newtonian nanofluids embedded with graphene nanoparticles. Advanced Powder Technology. 2016; 27(6): 2448-56. Doi: 10.1016/j.apt.2016.08.023
36. Sandeep N, Sharma RP, Ferdows M. Enhanced heat transfer in unsteady magnetohydrodynamic nanofluid flow embedded with aluminum alloy nanoparticles. Journal of Molecular Liquids. 2017; 234: 437-43. Doi: 10.1016/j.molliq.2017.03.051
37. Daniel YS, Aziz ZA, Ismail Z, Salah F. Impact of thermal radiation on electrical MHD flow of nanofluid over nonlinear stretching sheet with variable thickness. Alexandria Engineering Journal. 2018; 57(3): 2187-97. Doi: 10.1016/j.aej.2017.07.007
38. Maleki H, Safaei MR, Alrashed AA, Kasaeian A. Flow and heat transfer in non-Newtonian nanofluids over porous surfaces. Journal of Thermal Analysis and Calorimetry. 2019; 135: 1655-66. Doi: 10.1007/s10973-018-7277-9
39. Lin Y, Zheng L, Zhang X, Ma L, Chen G. MHD pseudo-plastic nanofluid unsteady flow and heat transfer in a finite thin film over stretching surface with internal heat generation. International Journal of Heat and Mass Transfer. 2015; 84: 903-11. Doi: 10.1016/j.ijheatmasstransfer.2015.01.099
40. Darbari B, Ayani MB. Heat transfer and deposition analysis of CuO-Water nanofluid inside a baffled channel: Two-phase Eulerian–Lagrangian method. Journal of the Taiwan Institute of Chemical Engineers. 2023: 104827. Doi: 10.1016/j.jtice.2023.104827
41. Wen D, Zhang L, He Y. Flow and migration of nanoparticle in a single channel. Heat and Mass Transfer. 2009; 45: 1061-7. Doi: 10.1007/s00231-009-0479-8
42. Soltani M, Ahmadi G. On particle adhesion and removal mechanisms in turbulent flows. Journal of Adhesion Science and Technology. 1994; 8(7): 763-85. Doi: 10.1163/156856194X00799
43. Brach RM, Dunn PF. A mathematical model of the impact and adhesion of microsphers. Aerosol Science and Technology. 1992; 16(1): 51-64. Doi: 10.1080/02786829208959537
44. Ounis H, Ahmadi G, McLaughlin JB. Brownian diffusion of submicrometer particles in the viscous sublayer. Journal of Colloid and Interface Science. 1991; 143(1): 266-77. Doi: 10.1016/0021-9797(91)90458-K
45. Husain A, Kim K-Y, editors. Microchannel heat sinking: analysis and optimization. Fluid Machinery and Fluid Mechanics: 4th International Symposium (4th ISFMFE); 2009: Springer. Doi: 10.1007/978-3-540-89749-1_25
46. Xia G, Chai L, Wang H, Zhou M, Cui Z. Optimum thermal design of microchannel heat sink with triangular reentrant cavities. Applied Thermal Engineering. 2011; 31(6-7): 1208-19. Doi: 10.1016/j.applthermaleng.2010.12.022
47. Kim D, Kwon Y, Cho Y, Li C, Cheong S, Hwang Y, Lee J, Hong D, Moon S. Convective heat transfer characteristics of nanofluids under laminar and turbulent flow conditions. Current Applied Physics. 2009; 9(2): e119-e23. Doi: 10.1016/j.cap.2008.12.047
48. Bali R, Awasthi U. Effect of a magnetic field on the resistance to blood flow through stenotic artery. Applied Mathematics and Computation. 2007; 188(2): 1635-41. Doi: 10.1016/j.amc.2006.11.019

Persian Abstract

چکیده

ته‌نشینی ذرات در میکروکانال ها از موضوعات مهمی است که تاثیر منفی بر انتقال حرارت نانوسیالات می‌گذارد. در این مطالعه رویکرد جدید استفاده از میدان مغناطیسی ناشی از سیم حامل جریان را برای جلوگیری از ته نشینی ذرات و افزایش انتقال حرارت با استفاده از مدل اویلری- لاگرانژی ارائه می‌کند. در این بررسی، معادلات جفت شده دوطرفه برای مومنتوم و انرژی، همراه با حضور نیروهایی مانند براونی، ترموفورسیس، پسا و نیروهای حجمی به کار گرفته شده است تا مکانیزم‌های ته‌نشینی ذرات و انتقال حرارت در هندسه های دوبعدی مختلف بررسی شود. نتایج نشان می‌دهد که تغییرات دما تجربه شده توسط ذرات ، خارج از لایه مرز حرارتی و تحت شرایط مورد بررسی در این مقاله تاثیر کمی نسبت به ذرات داخل لایه مرزی دارد که می‌تواند در بهینه سازی میزان مصرف نانوذرات موثر باشد. به علاوه، جریان با سرعت غیر توسعه یافته در ورودی میکروکانال، ته نشینی ذرات کمتری را در مقایسه با سرعت توسعه یافته ایجاد می کند. با توجه به نتایج، افزایش عدد رینولدز از ۵۰ تا ۳۰۰ منجر به افزایش ۱/۷۵ درصد فاصله ذرات از دیوار میکروکانال می شود که باعث کاهش ته‌نشینی ذرات می‌شود. همچنین حضور سیم حامل جریان در ابتدای میکروکانال با ایجاد نیروی هم جهت با بردار نرمال سطح باعث کاهش قابل توجهی در میزان ته نشینی ذرات در میکروکانال ها می‌گردد، به‌طوری‌که با افزایش جریان الکتریکی تا ۴ آمپر، راندمان عدم ته‌نشینی ذرات در میکروکانال به ۱۰۰٪ می‌رسد.